Combined excitation of running space charge and conductivity gratings in photorefractive crystals

Mikhail Bryushinin,* Vladimir Kulikov, and Igor Sokolov
A.F. Ioffe Physical Technical Institute, 194021, St. Petersburg, Russia
(Received 21 September 2004; revised manuscript received 27 December 2004; published 25 April 2005)

We report the simultaneous combined excitation of the space charge and photoconductivity gratings in photorefractive $Bi_{12}SiO_{20}$ and $Bi_{12}TiO_{20}$ crystals. The experiments are carried out using the light diffraction and non-steady-state photo-emf techniques. The crystal illumination with an oscillating interference pattern excites the running photoconductivity grating which interacts with the ac component of the applied field and gives rise to the space charge wave. Being the eigenmode of the space charge dynamics the wave reveals itself as the low-frequency resonant maximum at the frequency transfer function of the detected signals. The theory of the observed effects is constructed for the conventional one-level model of semiconductor with monopolar photoconductivity. The drift mobilities of electrons are estimated for *n*-type photorefractive $Bi_{12}SiO_{20}$ and $Bi_{12}TiO_{20}$ crystals: $\mu=(1.1-1.4)\times10^{-2}$ cm^2/V s ($Bi_{12}SiO_{20}$, $\lambda=532$ nm, $T=296-298$ K), $\mu=1.5\times10^{-2}$ cm^2/V s ($Bi_{12}SiO_{20}$, $\lambda=442$ nm, $T=293$ K), and $\mu=3.1\times10^{-3}$ cm^2/V s ($Bi_{12}TiO_{20}$, $\lambda=532$ nm, $T=293$ K).

DOI: 10.1103/PhysRevB.71.165208 PACS number(s): 72.20.Jv, 42.70.Nq

I. INTRODUCTION

The evolution of photoinduced charge in semiconductor materials mainly occurs in two basic stages: formation of the photoconductivity distribution and creation of the space charge.[1,2] For the crystal placed in an external electric field the relaxation of photoconductivity and space charge distributions has complex behavior (oscillation and running character).[3] The existence of two eigenmodes (branches) of space charge oscillation was predicted in Ref. 4. One of these eigenmodes describe oscillation of the space charge trapped on the local levels, while the other is associated with the oscillation of the density of electrons in the conduction band (conduction electrons). The former branch is historically called "space charge wave." To avoid the complexity we shall use the term "running grating of the conductivity" for the latter one. The dispersion laws of these waves—i.e., dependences of the temporal oscillation frequency on the spatial frequency K—can be written as follows:

$$\omega_{sc} = (\tau_M K L_0)^{-1}, \tag{1}$$

$$\omega_{pc} = K\mu E_0, \tag{2}$$

where τ_M is the Maxwell relaxation time, μ is the mobility, and L_0 is the drift length of electrons in dc electric field E_0. A number of approaches for investigations of the running space charge and conductivity gratings has been realized by the present time.[5–16]

In spite of the large number of publications dedicated to the subject of space charge waves the question of simultaneous excitation and interaction of the eigenmodes mentioned above is still unsolved. Most of the proposed optical techniques use the interference pattern with the specified spatial frequency K and temporal frequency ω for the excitation of either space charge wave or running photoconductivity grating. This is due to the fact that the eigenfrequency of space charge oscillations in high-resistive crystals (such as $Bi_{12}SiO_{20}$) is in the range $\omega_{sc}/2\pi=10-100$ Hz while the eigenfrequency of the photoconductivity grating with the same spatial period can reach considerably higher values: $\omega_{pc}/2\pi=0.01-1$ MHz. The situation is partly similar to the light scattering on the acoustic waves where interaction of particles with comparable momenta (wave vectors) and completely different energies (frequencies) takes place.

As is known from the oscillation theory, the behavior of systems with two degrees of freedom has distinctive features with respect to the one in systems with one degree of freedom. These features result in such effects as incoherent parametric amplification, generation, wideband parametric frequency division, etc. Considering two eigenmodes of space charge oscillations in photorefractive media one can expect some analogs in holographic recording.

For the realization of the simultaneous excitation and interaction of the space charge wave (ω_{sc},K) traveling along the dc electric field with the velocity ω_{sc}/K and electron conductivity grating $(\omega_{pc},-K)$ running in the opposite direction with velocity $-\omega_{pc}/K$ the third oscillation $(\Omega,0)$ satisfying the conditions analogous to the energy and momentum conservation laws is required: $\omega_{sc}+\omega_{pc}=\Omega$, $K-K=0$. The electric field with frequency Ω can play the role of such oscillation and provide necessary coupling.

In this paper we shall study one of the possible manifestations of this phenomenon: namely, the excitation of the space charge wave provided by the interaction of the running photoconductivity grating with an applied ac electric field. The effect is observed and investigated using optical[17] and electrical[18] methods. The first one is based on light diffraction on photorefractive volume holograms; the second one uses the non-steady-state photoelectromotive force effect[15,16] (nonstationary holographic photocurrent).

II. THEORETICAL ANALYSIS

For calculation of the space charge and conductivity distributions suppose the photorefractive crystal placed in exter-

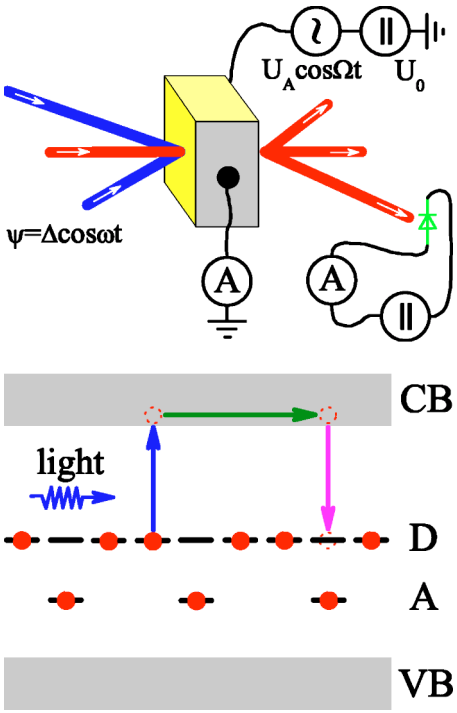

FIG. 1. (Color online) Scheme for observation of the combined excitation of running space charge and conductivity gratings (top). The model of semiconductor with the electron photoconductivity and one type of the partially compensated donor centers (bottom).

nal dc and ac electric fields is illuminated by the interference pattern formed by two plain light waves one of which is phase modulated (Fig. 1):

$$I(x,t) = I_0[1 + m\cos(Kx + \Delta\cos\omega t)]. \tag{3}$$

Here I_0, m, and K are the average light intensity, contrast, and spatial frequency of the interference pattern, and Δ and ω are the amplitude and frequency of phase modulation. The external dc and sinusoidal ac voltages applied to the crystal can be presented as follows:

$$U_{ext} = U_0 + U_A\cos\Omega t. \tag{4}$$

We consider the widely used model of semiconductor with monopolar photoconductivity and one type of partially compensated donor levels (Fig. 1).[1,2] The illumination provides generation of electrons from donor levels to the conduction band where they move due to the diffusion or drift mechanisms and recombine back. The concentration of electrons in the conduction band n changes in accordance with the balance equation

$$\frac{\partial n}{\partial t} = g - \frac{n}{\tau} + \frac{1}{e}\frac{\partial j_e}{\partial x}, \tag{5}$$

where $g(x,t)=(\alpha\beta/h\nu)I(x,t)$ is the electron generation rate (α is the light absorption coefficient, β is the quantum efficiency, $h\nu$ is the photon energy), τ is the electron lifetime, j_e is the density of the electron current, and e is the electron charge. It should be noted here that we consider the density of trapping centers to be independent of the experimental conditions (τ=const). This assumption means that we neglect the trap saturation effects, and it restricts the values of electric field and spatial frequency: $E_0 < E_q = eN_A/\epsilon\epsilon_0 K$, where N_A is the density of traps, ϵ is the dielectric constant, and ϵ_0 is the free space permittivity.[2,3] The electrons nonuniformly captured at donor levels produce the space charge density ρ and corresponding electric field E distributions:

$$\epsilon\epsilon_0\frac{\partial E}{\partial x} = \rho. \tag{6}$$

The density of space charge varies due to electron transport, and this process is governed by the continuity equation

$$\frac{\partial \rho}{\partial t} + \frac{\partial j_e}{\partial x} = 0. \tag{7}$$

The electron current j_e is defined by the drift and diffusion components:

$$j_e = e\mu nE + k_B T\mu\frac{\partial n}{\partial x}, \tag{8}$$

where μ is the electron mobility, k_B is the Boltzmann constant, and T is the temperature. Equations (5)–(8) can be rewritten in the form convenient for further analysis:[19]

$$\frac{\partial n}{\partial t} = g - \frac{n}{\tau} - \frac{\epsilon\epsilon_0}{e}\frac{\partial^2 E}{\partial x\partial t}, \tag{9}$$

$$-\frac{\epsilon\epsilon_0}{e}\frac{\partial^2 E}{\partial x\partial t} = \mu\frac{\partial}{\partial x}(nE) + \frac{k_B T}{e}\mu\frac{\partial^2 n}{\partial x^2}. \tag{10}$$

In the general case the solution of this set of equations is difficult, so let us suppose the contrast of the interference pattern and amplitude of phase modulation to be small ($m,\Delta \ll 1$). This will allow us to linearize the equations and to search the solution for $n(x,t)$, $E(x,t)$ distributions as the sums of stationary and running gratings:

$$n = n_0 + \sum_{p,q=-1}^{1} n^{+pq}\exp\{i[Kx + (p\omega + q\Omega)t]\} + \sum_{p,q=-1}^{1} n^{-pq}\exp\{i[-Kx + (p\omega + q\Omega)t]\}, \tag{11}$$

$$E = E_0 + \frac{E_A}{2}\exp(i\Omega t) + \frac{E_A}{2}\exp(-i\Omega t) + \sum_{p,q=-1}^{1} E^{+pq}\exp\{i[Kx + (p\omega + q\Omega)t]\} + \sum_{p,q=-1}^{1} E^{-pq}\exp\{i[-Kx + (p\omega + q\Omega)t]\}. \tag{12}$$

For the complex amplitudes with indices "+1" and "−1" we shall also use the notations with indices "+" and "−"—e.g., $n^{+(+1)(-1)} = n^{++-}$. The values E_0 and E_A are defined as corresponding voltage amplitudes divided by the value of interelectrode spacing L: $E_0 = U_0/L$ and $E_A = U_A/L$. We assume

that both the electrodes are Ohmic and the inhomogeneity of electric field in the volume is negligible.

Let us analyze the case of a "relaxation-type" semiconductor:

$$\tau \ll \tau_M. \tag{13}$$

Note that the opposite case (i.e., $\tau \gg \tau_M$) is slightly more complicated for the analysis. However, the application of strong electric fields decreases the time constant of the conductivity relaxation and increases the buildup time of the space charge, so we obtain conditions analogous to the "relaxation-type" regime.

Let us consider the "long-drift-length" regime of holographic recording:

$$KL_0 \gg 1 + K^2L_D^2, \tag{14}$$

where $L_0=\mu\tau E_0$ and $L_D=(k_BT\mu\tau/e)^{1/2}$ are the drift and diffusion lengths of photocarriers. This assumption is rather typical for theoretical considerations of various phenomena in photorefractive media: it ensures the oscillatory relaxation of the space charge and photoconductivity for large applied dc fields (in contrast to the exponential one in the diffusion regime).[2]

In this paper we shall develop two approaches. In the former one the frequency of an ac electric field is equal to the eigenfrequency of photoconductivity oscillation, and the difference frequency lies in the range of the space-charge-wave excitation:

$$\Omega = \omega_{pc}, \tag{15}$$

$$|\omega - \Omega| \sim \omega_{sc}. \tag{16}$$

The complex amplitudes introduced in Eqs. (11) and (12) and necessary for further analysis have been calculated. Below the most interesting terms presenting gratings with spatial frequency K and oscillation frequency $\pm(\omega-\Omega)$ are given:

$$n^{++-} = \frac{-im\Delta}{8D_1} n_0(\omega-\Omega)\tau_M KL_A, \tag{17}$$

$$E^{++-} = \frac{-im\Delta}{8D_1} E_A, \tag{18}$$

$$n^{+-+} = \frac{i3m\Delta}{8D_2} n_0(\omega-\Omega)\tau_M KL_A, \tag{19}$$

$$E^{+-+} = \frac{-i3m\Delta}{8D_2} E_A, \tag{20}$$

where

$$D_1 = (1+K^2L_D^2)[1+(\omega-\Omega)\tau_M KL_0] - i[(1+K^2L_D^2)^2 + K^2L_A^2/4]/KL_0, \tag{21}$$

$$D_2 = (1+K^2L_D^2)[5-11(\omega-\Omega)\tau_M KL_0] - i6KL_0[1-(\omega-\Omega)\tau_M KL_0], \tag{22}$$

and $L_A=\mu\tau E_A$.

The latter approach implies that frequencies of phase modulation and external field vary in the region of the photoconductivity grating oscillation maintaining the difference frequency constant and equal to the frequency of the space charge oscillation:

$$\omega, \Omega \sim \omega_{pc}, \tag{23}$$

$$\omega - \Omega = -\omega_{sc}. \tag{24}$$

The choice of negative sign in the right-hand side of Eq. (24) will be clear below when we shall analyze the frequency characteristics of the non-steady-state photo-emf and diffraction efficiency.

The corresponding complex amplitudes of electron density and electric field are the following:

$$n^{++-} = -\frac{m\Delta}{8D_3} n_0 KL_A[1+K^2L_D^2 + i(2\omega\tau - KL_0)], \tag{25}$$

$$E^{++-} = \frac{m\Delta}{8D_3} E_0 KL_A[1+K^2L_D^2 + i(2\omega\tau - KL_0)], \tag{26}$$

where

$$D_3 = (1+K^2L_D^2)[(1+K^2L_D^2)^2 + K^2L_A^2/2 - K^2L_0^2 + 3\omega\tau KL_0 - 2\omega^2\tau^2] + i[(1+K^2L_D^2)^2(3\omega\tau - 2KL_0) + K^2L_A^2(2\omega\tau - KL_0)/4]. \tag{27}$$

Let us now proceed with the calculation of the non-steady-state photo-emf and diffraction efficiency amplitudes—values which will be measured in the experiment. As was shown in Ref. 15 the non-steady-state photo-emf in crystal biased by voltage source is defined by the averaged drift component of the photocurrent:

$$j(t) = \frac{1}{L}\int_0^L e\mu n(x,t)E(x,t)dx. \tag{28}$$

As seen from Eqs. (11), (12), and (28) the signal with frequency $\omega-\Omega$ is produced by the following combination:

$$j^{\omega-\Omega}(t) = \mathrm{Re}\{2e\mu(n^{++-}E^{-00} + n^{-00}E^{++-} + n^{--+}E^{+00} + n^{+00}E^{-+-} + n^{++0}E^{-0-} + n^{-0-}E^{++0} + n^{-+0}E^{+0-} + n^{+0-}E^{-+0}) \times \exp[i(\omega-\Omega)t]\}. \tag{29}$$

The different nature of the items in this expression should be pointed out. The first four components are associated with the resonant excitation of the space charge waves with temporal frequency $\omega-\Omega$. The last four components in Eq. (29) are just mixing of the "fast" gratings with temporal frequencies ω and Ω. It is reasonable to expect that the former group produces larger contribution to the total current. This supposition is proved by the numerical calculation. Substituting the calculated above terms (17)–(20) into Eq. (29) we can write

down the expression for the complex amplitude of the nonstationary photocurrent as

$$j^{\omega-\Omega} \simeq -i\frac{m^2\Delta}{8}\sigma_0 E_A\left[\frac{1-(\omega-\Omega)\tau_M KL_0}{D_1} - 3\frac{1+(\omega-\Omega)\tau_M KL_0}{(D_2)^*}\right]. \quad (30)$$

The frequency transfer function of the non-steady-state photo-emf—i.e., the dependence $j^{\omega-\Omega}(\omega-\Omega)$—has two resonant maxima at $\omega-\Omega \simeq \pm\omega_{sc}$. The amplitudes of the resonant maxima at $\omega-\Omega=-\omega_{sc}$ and at $\omega-\Omega=\omega_{sc}$ are the following:

$$j_{r1}^{\omega-\Omega} \simeq \frac{m^2\Delta}{4}\frac{\sigma_0 E_A KL_0}{(1+K^2L_D^2)^2+K^2L_A^2/4}, \quad (31)$$

$$j_{r2}^{\omega-\Omega} \simeq -i\frac{m^2\Delta}{8}\frac{\sigma_0 E_A}{1+K^2L_D^2}. \quad (32)$$

The resonant maximum for the negative frequency difference is approximately $2KL_0$ times larger than for positive frequency difference. This fact is associated with the principal distinction in the physical mechanism of grating's excitation in these frequency regions.

For the negative frequency difference range $(\omega-\Omega<0)$ the space charge wave is originated from the interaction of an external field with the photoconductivity grating propagating in the direction opposite to the dc field. When the oscillations of the interference pattern are synchronized with the movement of drifting electrons the resonant enhancement of the photoconductivity grating takes place. Thus the simultaneous generation of the running space charge and photoconductivity gratings, which are the eigenwaves in this case, should be observed.

For positive frequency difference $(\omega-\Omega>0)$ the space charge wave arises due to the interaction of the external field with the conductivity grating driven in the direction of the dc field. The photoconductivity grating is not an eigenmode of semiconductor in this case. It just follows the movements of the oscillating interference pattern in the direction of dc field.

The diagram illustrating the interaction of the space charge and photoconductivity gratings with the applied ac field is presented in Fig. 2. As seen from the figure in the former case the applied ac field couples two eigenmodes of semiconductor satisfying the equations $\omega_{sc}+\omega_{pc}=\Omega$, $K-K=0$. In the latter case the only eigenmode—namely, the space charge wave—is excited. The fulfillment of the resonant conditions for both the space charge wave and photoconductivity grating ensures observation of larger signal's amplitudes.

The dependence $j^{\omega-\Omega}(\omega)$ with the fixed frequency difference $\omega-\Omega$ [Eqs. (23) and (24)] can be measured in the experiment as well. Direct substitution of Eqs. (25) and (26) into Eq. (29) gives the following expression for this dependence:

$$j^{\omega-\Omega} \simeq \frac{m^2\Delta}{4D_3}\sigma_0 E_A KL_0[1+K^2L_D^2+i(2\omega\tau-KL_0)]. \quad (33)$$

The analysis of the denominator in this expression [see Eq. (27)] revealed that the resonant maximum can be observed at

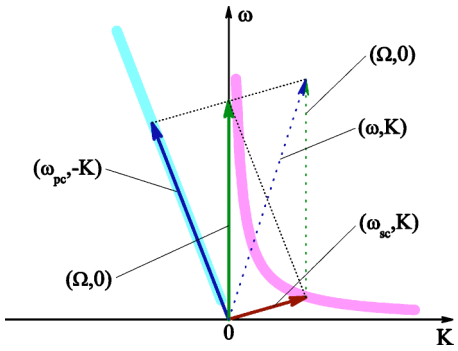

FIG. 2. (Color online) Diagram illustrating the interaction of running space charge and conductivity gratings with applied ac electric field. The arrows show the space charge grating (ω_{sc},K) traveling with the velocity ω_{sc}/K along the dc field, the photoconductivity grating $(\omega_{pc},-K)$ running with the velocity $-\omega_{pc}/K$ in the opposite direction, the photoconductivity grating (ω,K) driven with the velocity ω/K along the dc field, and the external ac field $(\Omega,0)$ with frequency Ω. The half-tone lines show the dispersion laws for the space charge wave $\omega_{sc}(K)$ and running photoconductivity grating $\omega_{pc}(-K)$.

$\omega \simeq \omega_{pc}$ and its amplitude is expressed by Eq. (31). This resonant peculiarity can be explained as follows: since the excited space charge oscillations at combination frequency are due to the interaction of the external ac electric field and the photoconductivity grating, the amplitude of the latter should affect the detected signal amplitude. The photoconductivity grating is resonantly excited at $\omega=\omega_{pc}$. So the resonant dependence of the low-frequency signal $j^{\omega-\Omega}$ versus phase modulation frequency ω (or the frequency of an ac electric field Ω) can be expected as well.

The diffraction efficiency of thin phase hologram recorded in photorefractive crystal equals

$$\eta(t) = |\pi n_p^3 r E^+(t) d/\lambda_p|^2, \quad (34)$$

where n_p and r are the refractive index and electro-optic coefficient of the crystal for wavelength λ_p of the probe readout light, $E^+(t)$ is the complex amplitude of $+K$ spatial component of the electric field, and d is the thickness of the crystal. The oscillations of the diffraction efficiency with frequency $\omega-\Omega$ are produced by the following components:

$$\eta^{\omega-\Omega}(t) = \mathrm{Re}\{2q^2[(E^{+00})^*E^{++-}+E^{+00}(E^{+-+})^*+(E^{+0+})^*E^{++0} + E^{+0-}(E^{+-0})^*]\exp[i(\omega-\Omega)t]\}; \quad (35)$$

here, $q=\pi n_p^3 r d/\lambda_p$. One can note the difference between two first and two last terms of the expression—similar to the ones mentioned above for the nonstationary photocurrent analysis. Direct substitution of Eqs. (18) and (20) into Eq. (35) provides the expression for the complex amplitude of the diffraction efficiency:

$$\eta^{\omega-\Omega} \simeq i\frac{m^2\Delta}{8}q^2 E_0 E_A\left[\frac{1}{D_1}-\frac{3}{(D_2)^*}\right]. \quad (36)$$

This frequency transfer function has two resonant maxima. The oscillation amplitudes of the diffraction efficiency at

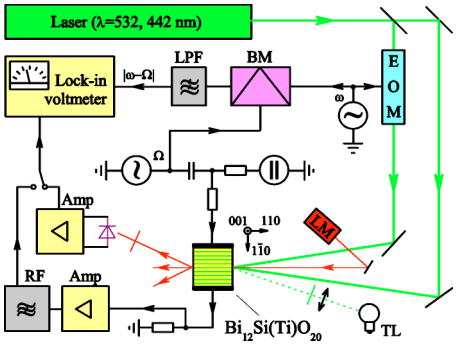

FIG. 3. (Color online) Experimental setup for the investigation of the combined excitation of space charge and photoconductivity gratings using the diffraction and non-steady-state photo-emf techniques. *EOM* is the electro–optic modulator, *LM* is the laser diode module (λ_p=650 nm), *TL* is the tungsten lamp, BM is the balance mixer, *Amp* are the amplifiers, and *LPF* and *RF* are the low-pass and rejection filters, respectively.

resonant frequencies $\omega-\Omega=-\omega_{sc}$ and $\omega-\Omega=\omega_{sc}$ are the following:

$$\eta_{r1}^{\omega-\Omega} \simeq -\frac{m^2\Delta}{8}\frac{q^2E_0E_AKL_0}{(1+K^2L_D^2)^2+K^2L_A^2/4}, \tag{37}$$

$$\eta_{r2}^{\omega-\Omega} \simeq i\frac{m^2\Delta}{16}\frac{q^2E_0E_A}{1+K^2L_D^2}. \tag{38}$$

Like in Eqs. (31) and (32) these resonant peaks differ by factor of $\sim 2KL_0$ due to the same reason: the simultaneous excitation of two eigenmodes is more efficient.

The dependence of the diffraction efficiency amplitude $\eta^{\omega-\Omega}$ on the frequency of phase modulation, ω, with fixed difference frequency $\omega-\Omega=-\omega_{sc}$ can be calculated substituting Eq. (26) into Eq. (35):

$$\eta^{\omega-\Omega} \simeq -\frac{m^2\Delta}{8D_3}q^2E_0^2KL_A[1+K^2L_D^2+i(2\omega\tau-KL_0)]. \tag{39}$$

The resonant maximum with amplitude (37) is observed at frequency $\omega\simeq\omega_{pc}$.

This frequency dependence along with the signal dependence of the non-steady-state photo-emf effect [Eq. (33)] can be utilized for direct measurements of the photocarrier's drift mobility $\mu=\omega_{pc}/KE_0$.

We have considered here the simplest case of thin hologram recorded in slightly absorbing media. The generalization of the theory for the cases of thick holograms in absorbing and optically active materials can be done as required using the approaches known in literature.[2,3,20]

III. EXPERIMENTAL SETUP

The scheme of the experimental setup for the investigation of the combined excitation of space charge and conductivity gratings in photorefractive crystals using the light diffraction technique is presented in Fig. 3. The experiments were performed in *n*-type photorefractive $Bi_{12}SiO_{20}$ and $Bi_{12}TiO_{20}$ crystals. The crystals were grown under conventional conditions; they were not specially doped. However, the photorefractive $Bi_{12}TiO_{20}$ crystal contains $(3.0-4.2)\times10^{-4}$ wt % of chromium.[21,22] The typical sample dimensions were $9.2\times2.5\times2.5$ mm^3 ($Bi_{12}SiO_{20}$), $9.2\times2.5\times3.2$ mm^3 ($Bi_{12}TiO_{20}$). The crystals had one of the standard holographic orientation: the polished front and back surfaces (9.2×2.5 mm^2) were parallel to the plane (110) and electric field was applied along the $[1\bar{1}0]$ axis. The silver paste electrodes were painted on the lateral surfaces. The interelectrode spacings were equal to L=2.5 mm.

The second harmonic of the Nd:YAG laser was used as a source of coherent radiation (λ=532 nm, $P_{out}\simeq$10 mW). The laser light was split into two beams, one of which was phase modulated with frequency ω using an electro-optic modulator ML-102A. The amplitude of phase modulation was equal Δ=0.61. The light beams were expanded and directed on the crystal's surface where they formed oscillating interference pattern with an average intensity I_r =25 mW/cm^2, contrast m_r=0.98, and spatial frequency K =190 mm^{-1}. The crystal was placed in dc and ac electric voltages: $U_{ext}=U_0+U_A\cos\Omega t$. The presence of the dc voltage U_0 is the necessary condition for the generation of running gratings. The ac voltage with an amplitude U_A and frequency Ω couples running gratings of the space charge and conductivity.

The weak probe laser beam with intensity I_p =7 mW/cm^2 was produced by the laser diode module (λ_p =650 nm). The polarization of probe beam in the middle of the crystal was at 45° with respect to the $[1\bar{1}0]$ and [001] axes. The intensity oscillations of the diffracted probe beam were detected by the conventional photodiode connected to transimpedance amplifier. The output electrical signal was measured by the lock-in nanovoltmeter Unipan-232B (f =1.5×10^0–1.5×10^5 Hz, τ_{int}=1–100 s). The measurements were carried out at the difference combination frequency $|\omega-\Omega|$. The reference voltage with this frequency was formed in the balance mixer (K174PS1) via multiplication of voltages applied to the crystal and electro-optic modulator. The harmonics of the reference voltage with frequencies ω, Ω, and $\omega+\Omega$ were suppressed by the low-pass filter.

The light from a 100-W tungsten lamp was used for the increase of the total light intensity; additional illumination also decreased the contrast of the interference pattern. It was focused and filtered (λ_b=480–590 nm) and its intensity value was I_b=200 mW/cm^2. The total light intensity was equal to $I_0=I_r+I_b\simeq$230 mW/cm^2, while the contrast of the interference pattern was reduced to $m=m_rI_r/I_0$=0.11. The green light transmitted through the crystal was cut by the red filter ($\lambda_{KS\text{-}10}$=600–2700 nm). The crystal's temperature was measured with the PtRh-Pt thermocouple.

The investigation of the effect using the non-steady-state photo-emf technique was performed with the similar arrangement (Fig. 3). In this approach the non-steady-state photocurrent arising in the crystal's volume generates the corresponding voltage drop on the load resistor R_L=18 kΩ. Then this signal was amplified, filtered, and measured by the lock-in nanovoltmeter Unipan-232B. The He—Cd laser was

used as a source of coherent radiation ($\lambda = 442$ nm, $P_{out} \simeq 3$ mW). The interference pattern with an average intensity $I_0 = 8.4$ mW/cm^2, contrast $m = 0.92$, and spatial frequency $K = 25$ mm^{-1} has the amplitude of phase modulation $\Delta = 0.8$. The measurements were carried out in photorefractive $Bi_{12}SiO_{20}$ without probe beam and additional illumination. The crystal's dimensions were $10 \times 3 \times 1$ mm^3. The front and back surfaces (10×1 mm^2) were polished to optical quality. The silver paste electrodes (3×3 mm^2) were painted on the lateral surfaces. The interelectrode spacing was equal to $L = 1$ mm. The sample was placed between two styrofoam linings in order to prevent mechanical oscillations due to piezoelectric effect.

In the experiments using standard diffraction and non-steady-state techniques[15,16] the only dc voltage U_0 was applied to the crystal, and the signal was detected at the frequency of phase modulation ω. The output signal was measured by spectrum analyzers SK4-56 ($f = 0.01-50$ kHz, $\Delta f = 3$ Hz), SK4-58 ($f = 0.4-600$ kHz, $\Delta f = 100$ Hz), and lock-in nanovoltmeter Unipan-232B.

IV. EXPERIMENTAL RESULTS

A. Diffraction measurements

For the determination of eigenfrequencies of space charge and conductivity oscillations let us discuss the results of the diffraction measurements in photorefractive $Bi_{12}SiO_{20}$ using standard technique of signal excitation.

The diffraction efficiency of the hologram was defined as $\eta = I_{p1}/I_p$, where I_{p1} is the intensity of the probe beam for the first order of diffraction. The diffraction efficiency of the stationary hologram recorded in the electric field $E_0 = U_0/L = 16$ kV/cm was equal to $\eta_0 = 2.0\%$. Figure 4 presents the frequency transfer function of the diffraction efficiency oscillations η^ω measured at frequency of phase modulation ω. The first resonant maximum is observed in the low-frequency range ($\omega/2\pi = 27-110$ Hz). When the electric field is increased the signal amplitude increases as well and the first maximum shifts to lower excitation frequencies (Fig. 4, inset). The shoulder at frequencies $\omega/2\pi = 10-50$ kHz was observed as well. Perhaps, for larger applied electric fields this shoulder could transfer into the second maximum, but field amplitudes $E_0 > 8$ kV/cm shift this shoulder beyond the investigated frequency range. The signal amplitude at $\omega/2\pi > 50$ kHz was so small that utilization of spectrum analyzer with appropriate frequency range and larger detection bandwidth (SK4-58) was not successful.

For this reason we used another approach based on the non-steady-state photo-emf measurements. The frequency transfer function of the non-steady-state photo-emf signal excited in $Bi_{12}SiO_{20}$ crystal is presented in Fig. 5. Two resonant maxima on the frequency dependences were observed. The increase of an applied field amplitude shifts the first and second maxima to the low- and high-frequency bands, respectively (Fig. 5, inset). As was shown in Ref. 16 such signal behavior is associated with the resonant excitation of running gratings of the space charge and conductivity described by the dispersion laws (1) and (2). Note that the first

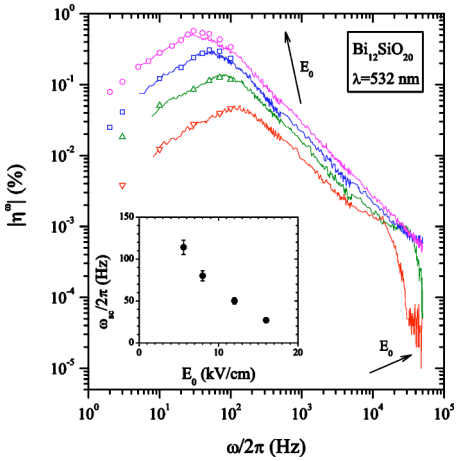

FIG. 4. (Color online) Frequency transfer functions of the diffraction efficiency oscillations excited in $Bi_{12}SiO_{20}$ at the frequency of phase modulation ω (standard technique, $E_A = 0$). The dependences are measured for four values of the applied dc electric field: $E_0 = 5.6$ kV/cm (▽), 8.0 kV/cm (△), 12 kV/cm (□), and 16 kV/cm (○). The measurements performed using spectrum analyzer and lock-in voltmeter are presented by the solid lines and symbols, respectively. The arrows show the directions of curve evolution with increasing field amplitude E_0. The inset presents the dependence of the first resonant frequency on the applied dc field.

resonant maximum is wide; this can be due to nonlinearity of the space charge formation for large contrast of the interference pattern.[23]

The non-steady-state photo-emf technique provides the unique opportunity for the direct determination of the photocarrier drift mobility. The value of the second resonant frequency measured for the specified K and E_0 is associated

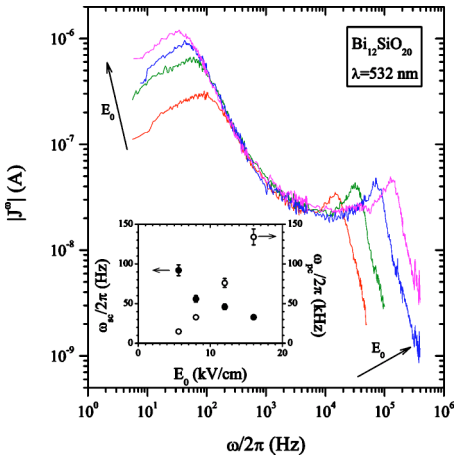

FIG. 5. (Color online) Frequency transfer functions of the non-steady-state photo-emf excited in $Bi_{12}SiO_{20}$ versus frequency of phase modulation ω (standard technique, $E_A = 0$). The dependences are measured for four values of the applied dc electric field: $E_0 = 5.6, 8.0, 12, 16$ kV/cm. The arrows shows the directions of curve evolution with increasing field E_0. Dependences of the first (●) and second (○) resonant frequencies versus applied dc field are presented in the inset.

TABLE I. Drift mobility of electrons in $Bi_{12}SiO_{20}$ crystal estimated from the frequency transfer function of the non-steady-state photo-emf $|J^{\omega}(\omega)|$.

E_0 (kV/cm)	T (K)	μ (cm^2/V s)
5.6	294	0.89×10^{-2}
8.0	296	1.4×10^{-2}
12	298	2.1×10^{-2}
16	300	2.8×10^{-2}

with the electron mobility value (Table I). The obtained data are in good agreement with the values measured earlier.[16,24,25]

The preliminary experiments allowed us to estimate corresponding resonant frequencies which can be used for further analysis of the simultaneous generation of the space charge and photoconductivity gratings.

For the realization of such regime the frequency of the external ac field was settled to be approximately equal to the frequency of the second resonant maximum. Small deviations (0.3–1.0 kHz) of frequency $\Omega/2\pi$ from the resonant frequency value $\omega_{pc}/2\pi$ are acceptable since the width of the second resonant maximum reaches 15–130 kHz (see Fig. 5). The amplitude of an external ac electric field was chosen noticeably smaller than the value of the dc field ($E_A=U_A/L$ =1.4–5.6 kV/cm), so possible shifts of the resonant frequencies are expected to be negligible.

Figure 6 presents the frequency transfer function of the diffraction efficiency oscillations excited at a difference combination frequency $\omega-\Omega$. Two maxima were observed at this dependence: the first one at the negative difference frequency $(\omega-\Omega)/2\pi=-(100-33)$ Hz ($E_0=5.6$–16 kV/cm) and the second one at the positive frequency $(\omega-\Omega)/2\pi=40$ Hz ($E_0=16$ kV/cm). The increase of the external dc field leads to the growth of the signal amplitude and corresponding shift of the resonant maxima to lower frequencies. This behavior

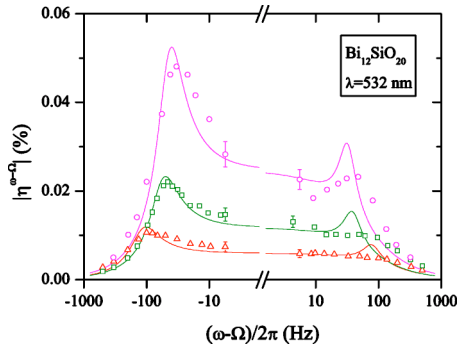

FIG. 6. (Color online) The frequency transfer function of the diffraction efficiency oscillations excited in $Bi_{12}SiO_{20}$ at the combination frequency $\omega-\Omega$. The dependences are obtained for three values of the applied dc field and for three corresponding frequencies of the applied ac field: $E_0=5.6$ kV/cm, $E_A=1.4$ kV/cm, $\Omega/2\pi=15$ kHz (△), $E_0=8.0$ kV/cm, $E_A=2.6$ kV/cm, $\Omega/2\pi=33$ kHz (□), and $E_0=16$ kV/cm, $E_A=5.6$ kV/cm, and $\Omega/2\pi=130$ kHz (○). The approximation of the experimental dependences by Eq. (36) is shown by the solid lines.

TABLE II. Material parameters used for approximation of the experimental dependences in Fig. 6 by Eq. (36).

E_0 (kV/cm)	E_A (kV/cm)	τ_M (ms)	$\mu\tau$ (cm^2/V)
5.6	1.4	0.83	1.8×10^{-7}
8.0	2.6	1.7	1.3×10^{-7}
16	5.6	1.8	7.2×10^{-8}

is the typical manifestation of the space charge waves.[2] The experimental curves are well fitted by Eq. (36) with the parameters presented in Table II. Different values of the maxima in the region of negative and positive difference frequencies is an important peculiarity of the frequency transfer function (Fig. 6). One can notice another feature: the values of the $\mu\tau$ product estimated from this frequency dependence noticeably decrease at large applied fields (Table II). In fact, decrease of the quality factor of the space charge wave is observed. This decrease is most probably due to effects of trap saturation and it is not associated with any decay of the $\mu\tau$ product. According to Ref. 26 trap saturation effects reduce quality factor at $E_0>[(N_A/\epsilon\epsilon_0)(e/K^2\mu\tau+k_BT)]^{1/2}$. For $Bi_{12}SiO_{20}$ crystal with $N_A\simeq10^{16}$ cm^{-3}, $\epsilon=56$, and $\mu\tau\simeq10^{-6}$ cm^2/V this reduction should appear at $E_0\simeq10$ kV/cm, which well corresponds to the observed behavior. The proper description of the effect in trap saturation regime can be done by the appropriate modification of the basic equation set [Eqs. (5)–(8)] and subsequent calculations.

The dependence of the diffraction efficiency $|\eta^{\omega-\Omega}|$ measured at negative combination frequency versus amplitude of the applied ac field E_A is presented in Fig. 7. This dependence seems to be linear in the region $E_A=0$–1.0 kV/cm. The higher fields cause the noticeable saturation of the signal amplitude. This behavior can be explained as follows. The interaction of the ac field with the running photoconductivity grating is more efficient for higher amplitudes of an ac field; this also results in the growth of space charge wave. However, large ac fields perturb the propagation of the photoconductivity grating. As is known,[16,25] the excitation of running photoconductivity gratings occurs when the moving light pattern is synchronized with the propagation of photocarriers drifting in dc electric field. Higher values of the applied ac

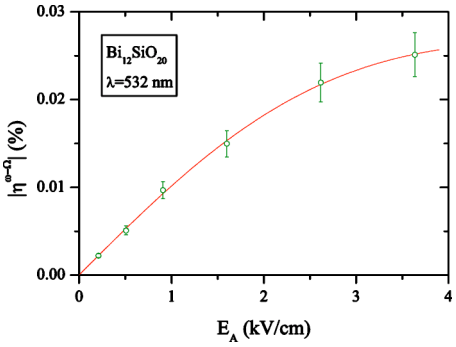

FIG. 7. (Color online) Dependence of the diffraction efficiency amplitude $|\eta^{\omega-\Omega}|$ versus amplitude of an ac electric field E_A. $Bi_{12}SiO_{20}$, $E_0=8.0$ kV/cm, $\Omega/2\pi=33$ kHz, and $(\omega-\Omega)/2\pi=-54$ Hz. The solid line shows the approximation by Eq. (37).

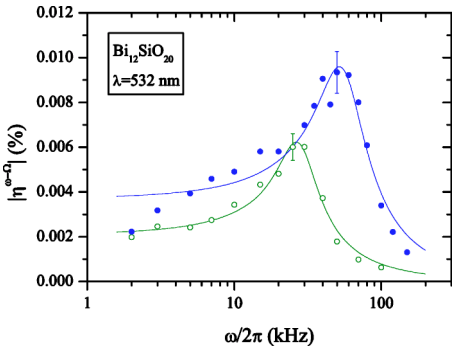

FIG. 8. (Color online) Dependence of the diffraction efficiency amplitude $|\eta^{\omega-\Omega}|$ versus frequency of phase modulation ω. The measurements are carried out for two values of dc field and corresponding combination frequencies: $E_0=8.0$ kV/cm, $(\omega-\Omega)/2\pi=-48$ Hz (○), $E_0=12$ kV/cm, and $(\omega-\Omega)/2\pi=-38$ Hz (●). $Bi_{12}SiO_{20}$, $E_A=0.92$ kV/cm. The approximation by Eq. (39) is shown by the solid lines.

field comparable with the dc bias lead to considerable change of drift velocities; the synchronization is partially lost, leading to the reduction of the running photoconductivity grating amplitude. This causes the saturation of the resulting space charge wave and corresponding detected signal. The obtained experimental dependence is approximated by Eq. (37) with $\mu\tau=2.1\times10^{-7}$ cm^2/V.

The dependence of the diffraction efficiency versus frequency of phase modulation $|\eta^{\omega-\Omega}(\omega)|$ was measured in $Bi_{12}SiO_{20}$ crystal for the constant combination frequency $\omega-\Omega\approx-\omega_{sc}$ (Fig. 8). The experimental curves demonstrate the behavior typical for running photoconductivity gratings: the growth of the dc electric field increases the amplitude of the detected signal and shifts the resonant peak to higher modulation frequencies (2). The resonant frequency values are slightly smaller than those obtained for the non-steady-state photo-emf experiments (Fig. 5). The approximation of the experimental dependences by Eq. (39) allowed determination of the drift mobility of electrons as well as the $\mu\tau$ product (Table III).

The mobility measurements were carried out in photorefractive $Bi_{12}TiO_{20}$ (Fig. 9). This crystal has sufficiently lower photoconductivity and corresponding resonant frequency of space charge oscillations, ω_{sc}. Thus the minimal possible combination frequency $(\omega-\Omega)/2\pi=-10$ Hz was settled close to the resonant frequency. The amplitude of the detected signal was significantly lower than the one in $Bi_{12}SiO_{20}$ crystal due to the same reason: the smaller conductivity grating excites weak space charge wave. The electron mobility and the $\mu\tau$ product were estimated from the

TABLE III. Material parameters of the $Bi_{12}SiO_{20}$ crystal estimated from the frequency dependence of the diffraction efficiency amplitude $|\eta^{\omega-\Omega}(\omega)|$.

E_0 (kV/cm)	T (K)	μ (cm^2/V s)	$\mu\tau$ (cm^2/V)
8.0	296	1.1×10^{-2}	1.9×10^{-7}
12	298	1.4×10^{-2}	1.1×10^{-7}

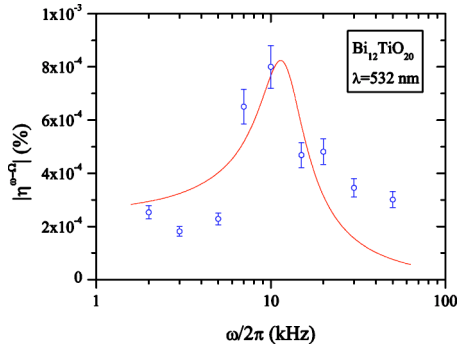

FIG. 9. (Color online) Dependence of the diffraction efficiency amplitude $|\eta^{\omega-\Omega}|$ versus frequency of phase modulation ω. $Bi_{12}TiO_{20}$, $E_0=12$ kV/cm, $E_A=0.92$ kV/cm, and $(\omega-\Omega)/2\pi=-10$ Hz. The solid line shows the approximation by Eq. (39).

frequency dependence (Fig. 9): $\mu=3.1\times10^{-3}$ cm^2/V s and $\mu\tau=1.4\times10^{-7}$ cm^2/V ($T=293$ K).

The obtained drift mobility values in $Bi_{12}SiO_{20}$ and $Bi_{12}TiO_{20}$ crystals are lower by 2–3 orders of magnitude than the actual band[27] and Hall[28] mobilities. Such difference is usually attributed to the process of strong trapping of photoelectrons on the shallow levels[24] or large polarons influence.[27]

B. Non-steady-state photo-emf measurements

In this subsection we consider the application of another—namely, the non-steady-state photo-emf technique for the detection of the discussed processes in $Bi_{12}SiO_{20}$ at $\lambda=442$ nm.

Figure 10 presents the frequency transfer functions of the non-steady-state photo-emf measured in $Bi_{12}SiO_{20}$ crystal for three values of the applied dc field E_0. If the value of an applied electric field is increased, the signal amplitude increases as well. Initially, the first resonant maximum appears in the low-frequency region ($\omega/2\pi\sim100$ Hz). When the dc field reaches $E_0\simeq6$ kV/cm the shoulder is observed on the frequency transfer function at $\omega/2\pi\sim3$ kHz. The further increase of an applied field amplitude transforms this shoulder

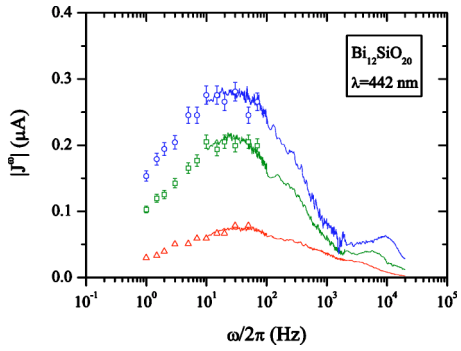

FIG. 10. (Color online) Frequency transfer functions of the non-steady-state photo-emf excited in $Bi_{12}SiO_{20}$. Standard technique ($E_A=0$). The dependences are measured for three values of the applied dc electric field: $E_0=6$ kV/cm (△), 10 kV/cm (□), and 14 kV/cm (○).

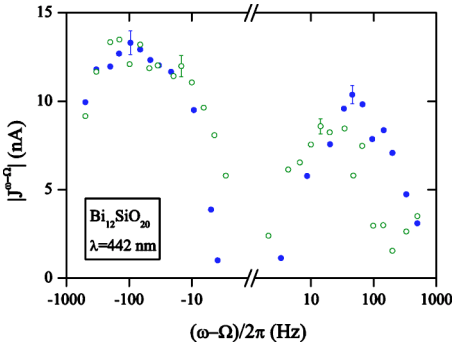

FIG. 11. (Color online) Frequency transfer function of the non-steady-state photo-emf excited in $Bi_{12}SiO_{20}$ by the combination technique. The dependences are obtained for two values of the applied dc field and for two corresponding frequencies of the applied ac field: $E_0=10$ kV/cm, $\Omega/2\pi=5.9$ kHz (○), $E_0=14$ kV/cm, and $\Omega/2\pi=8.8$ kHz (●). $E_A=3.5$ kV/cm.

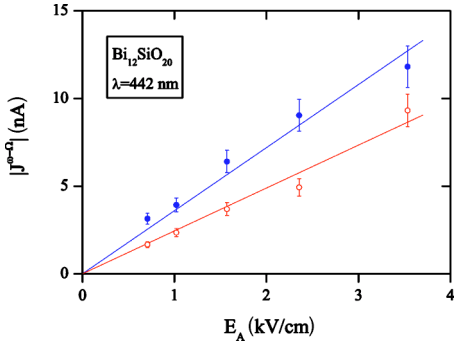

FIG. 12. (Color online) Dependence of the non-steady-state photo-emf amplitude $|J^{\omega-\Omega}|$ on the amplitude of the applied ac field. The measurements are carried out for two resonant frequencies: $(\omega-\Omega)/2\pi=-20$ Hz (●) and $(\omega-\Omega)/2\pi=+20$ Hz (○). $E_0=14$ kV/cm and $\Omega/2\pi=8.8$ kHz.

into the second resonant maximum. The growth of the applied field shifts the first and second maxima to lower- and higher-excitation-frequency regions, respectively. For example, the resonant frequencies equal $\omega_{sc}/2\pi\simeq 25$ Hz and $\omega_{pc}/2\pi\simeq 5.6$ kHz for the electric field $E_0=10$ kV/cm and $\omega_{sc}/2\pi\simeq 20$ Hz and $\omega_{pc}/2\pi\simeq 9.1$ kHz for the electric field $E_0=14$ kV/cm. It was shown[16] that such signal behavior is associated with the resonant excitation of the space charge and photoconductivity running gratings. The first resonance is very wide which can also be attributed to the nonlinear character of the space charge formation for large contrast of the interference pattern.[23] The light intensity inhomogeneity can be another reason for such behavior: strong light absorption ($\alpha\sim 30$ cm^{-1}) makes the space charge relaxation time in the surface layer smaller than in the crystal's bulk.

Direct measurements of the photocarrier's drift mobility were carried out using the non-steady-state photo-emf technique. The mobility value was estimated from the position of the second resonant frequency for fixed K and E_0 values: $\mu\simeq 0.015$ cm^2/V s. This estimation is in good agreement with an electron mobility value $\mu=0.016$ cm^2/V s measured earlier at the wavelength $\lambda=458$ nm.[16] Nevertheless, the large light absorption the parameters estimated from the high-frequency resonant maximum seem to be rather correct since the resonant frequency and the shape of the resonant peak are not defined by parameters dependent on light intensity [Eqs. (33) and (39)].

Let us proceed with the combined excitation of the space charge and photoconductivity gratings. The frequency of an external ac field was settled approximately equal to the frequency of the second resonant maximum: $\Omega/2\pi=5.9$ kHz for $E_0=10$ kV/cm and $\Omega/2\pi=8.8$ kHz for $E_0=14$ kV/cm. The amplitude of an external ac field ($E_A=3.5$ kV/cm) was chosen to be considerably smaller than the dc field value.

Figure 11 presents the frequency transfer function of the non-steady-state photo-emf excited at difference combination frequency $\omega-\Omega$. Two maxima are clearly seen at this dependence: the first one is observed for the negative difference frequency $(\omega-\Omega)/2\pi=-(50-200)$ Hz ($E_0=10$ kV/cm) and $(\omega-\Omega)/2\pi=-(20-200)$ Hz ($E_0=14$ kV/cm) and the second one for the positive frequency $(\omega-\Omega)/2\pi=50$ Hz ($E_0=10$ kV/cm) and $(\omega-\Omega)/2\pi=30$ Hz ($E_0=14$ kV/cm). The increase of the external dc field causes the growth of the signal amplitude as well as the shift of the resonant maxima to lower frequencies. This behavior is typical for the space charge waves.[2] The resonant maxima turned out to be wide. This fact can be attributed to the nonlinear limitation of the space charge field for large contrasts of the interference pattern. The inhomogeneity of the light distribution through the sample thickness can be another reason of such behavior.

Figure 12 presents the dependences of the non-steady-state photo-emf amplitude at resonant frequencies versus amplitude of the applied ac field. These dependences seem to be linear in the investigated range of ac field amplitudes. The saturation of the signal amplitude can be expected for such values of an ac field E_A when $KL_A\sim 2$ [see Eqs. (31) and (32)]. For $\mu\tau\sim 10^{-6}$ cm^2/V (see, for example, Ref. 19) and $K=25$ mm^{-1} this saturation effect should be observed for $E_A\sim 8$ kV/cm.

V. CONCLUSION

In this paper we have considered the combined excitation of two eigenmodes in semiconductor: the running gratings of the space charge and photoconductivity. The novel technique based on the diffraction efficiency measurements allowed us to detect the space charge wave originated from the nonlinear interaction of the running photoconductivity grating with the applied ac field.

The most important feature of this approach is the difference between the spatiotemporal characteristics of the arising space charge wave and the spatiotemporal characteristics of the external driving forces (illumination and applied field). In this sense, the experiments presented in the paper is another demonstration of the eigennature of the space charge wave—the oscillation which properties are defined by the material parameters rather than external forces.

The combined excitation of the photoconductivity and space charge waves is very promising for the investigation of fast processes in high-resistive semiconductors. The measurement of the actual drift mobility of photocarriers in

wide-gap semiconductors with complicated structure of recombination levels is an important example of the tasks, where detection of high-frequency signals is necessary. Indeed, the resonant frequency of the photoconductivity grating can reach 100 MHz in $Bi_{12}SiO_{20}$ crystal.[25] Due to the large values of Maxwell relaxation time ($\tau_M \sim 1$ ms), oscillations of the space charge field and corresponding diffraction efficiency should be negligible in this frequency range: the reduction coefficient is $(\omega\tau_M)^{-1}$. This makes observation of the high-frequency resonances practically impossible. In contrast to the standard techniques the developed approach of combined excitation allows the detection of fast processes in the low-frequency region.

The nonlinear interaction of applied ac field with running gratings of the photoconductivity and space charge is not restricted to the results obtained in this paper. Further experimental investigations in other wide-gap semiconductors should be carried out, and more detailed theoretical analyses including trap saturation, optical activity, and absorption effects should be performed to complete description of the phenomena discussed.

ACKNOWLEDGMENT

The authors acknowledge the financial support from a grant of the President of the Russian Federation (Grant No. MK-2744.2003.02).

*Electronic address: mb@mail.ioffe.ru

[1] S. M. Ryvkin, *Photoelectric Effects in Semiconductors* (Consultants Bureau, New York, 1964).
[2] M. P. Petrov, S. I. Stepanov, and A. V. Khomenko, *Photorefractive Crystals in Coherent Optical Systems* (Springer-Verlag, Berlin, 1991).
[3] L. Solymar, D. J. Webb, and A. Grunnet-Jepsen, *The Physics and Applications of Photorefractive Materials* (Clarendon Press, Oxford, 1996).
[4] R. F. Kazarinov, R. A. Suris, and B. I. Fuks, Sov. Phys. Semicond. **7**, 102 (1973).
[5] J. P. Huignard and A. Marrakchi, Opt. Commun. **38**, 249 (1981).
[6] S. I. Stepanov, V. V. Kulikov, and M. P. Petrov, Opt. Commun. **44**, 19 (1982).
[7] J. P. Partanen, J. M. C. Jonathan, and R. W. Hellwarth, Appl. Phys. Lett. **57**, 2404 (1990).
[8] G. Hamel de Montchenault, B. Loiseaux, and J. P. Huignard, Electron. Lett. **22**, 1030 (1986).
[9] J. M. Heaton and L. Solymar, IEEE J. Quantum Electron. **24**, 558 (1988).
[10] M. P. Petrov, V. M. Petrov, V. V. Bryksin, A. Gerwens, S. Wevering, and E. Krätzig, J. Opt. Soc. Am. B **15**, 1880 (1998).
[11] S. Mallick, B. Imbert, H. Ducollet, J. P. Herriau, and J. P. Huignard, J. Appl. Phys. **63**, 5660 (1988).
[12] H. C. Pedersen and P. M. Johansen, Opt. Lett. **20**, 689 (1995).
[13] M. P. Petrov, V. V. Bryksin, H. Vogt, F. Rahe, and E. Krätzig, Phys. Rev. B **66**, 085107 (2002).
[14] U. Haken, M. Hundhausen, and L. Ley, Phys. Rev. B **51**, 10579 (1995).
[15] M. P. Petrov, I. A. Sokolov, S. I. Stepanov, and G. S. Trofimov, J. Appl. Phys. **68**, 2216 (1990).
[16] I. A. Sokolov and S. I. Stepanov, J. Opt. Soc. Am. B **10**, 1483 (1993).
[17] M. Bryushinin, Appl. Phys. B: Lasers Opt. **79**, 851 (2004).
[18] M. A. Bryushinin, Zh. Tekh. Fiz. **74**, 62 (2004)[**49**, 1016 (2004)].
[19] M. Bryushinin, V. Kulikov, and I. Sokolov, Phys. Rev. B **65**, 245204 (2002).
[20] H. Kogelnik, Bell Syst. Tech. J. **48**, 2909 (1969).
[21] S. L. Sochava, E. V. Mokrushina, V. V. Prokof'ev, and S. I. Stepanov, J. Opt. Soc. Am. B **10**, 1600 (1993).
[22] Yu. B. Afanas'ev, E. V. Mokrushina, A. A. Nechitailov, and V. V. Prokof'ev, Tech. Phys. Lett. **23**, 181 (1997).
[23] S. Mansurova, S. Stepanov, N. Korneev, and C. Dibon, Opt. Commun. **152**, 207 (1998).
[24] S. L. Hou, R. B. Lauer, and R. E. Aldrich, J. Appl. Phys. **44**, 2652 (1973).
[25] M. A. Bryushinin and I. A. Sokolov, Phys. Rev. B **63**, 153203 (2001).
[26] B. I. Sturman, M. Mann, J. Otten, and K. H. Ringhofer, J. Opt. Soc. Am. B **10**, 1919 (1993).
[27] I. Biaggio, R. W. Hellwarth, and J. P. Partanen, Phys. Rev. Lett. **78**, 891 (1997).
[28] S. L. Sochava, K. Buse, and E. Krätzig, Phys. Rev. B **51**, 4684 (R) (1995).